Cancer Science
The official journal of the Japanese Cancer Association

Accumulated phosphatidylcholine (16:0/16:1) in human colorectal cancer; possible involvement of LPCAT4

Nobuya Kurabe,[1] Takahiro Hayasaka,[2] Mikako Ogawa,[3] Noritaka Masaki,[2] Yoshimi Ide,[2,3] Michihiko Waki,[2] Toshio Nakamura,[4] Kiyotaka Kurachi,[4] Tomoaki Kahyo,[1] Kazuya Shinmura,[1] Yutaka Midorikawa,[5] Yasuyuki Sugiyama,[6,7] Mitsutoshi Setou[2,8] and Haruhiko Sugimura[1,8]

Departments of [1]Tumor Pathology; [2]Cell Biology and Anatomy; [3]Surgery I (Breast Surgery); [4]Surgery II (Colorectal Surgery), Hamamatsu University School of Medicine, Shizuoka; [5]Department of Digestive Surgery, Nihon University School of Medicine, Tokyo; [6]Department of Surgery, Gifu Municipal Hospital, Gifu; [7]Department of Surgery, Teikyo University School of Medicine University Hospital, Kawasaki, Japan

(Received December 4, 2012/Revised June 17, 2013/Accepted June 22, 2013/Accepted manuscript online July 2, 2013/Article first published online July 30, 2013)

The identification of cancer biomarkers is critical for target-linked cancer therapy. The overall level of phosphatidylcholine (PC) is elevated in colorectal cancer (CRC). To investigate which species of PC is overexpressed in colorectal cancer, an imaging mass spectrometry was performed using a panel of non-neoplastic mucosal and CRC tissues. In the present study, we identified a novel biomarker, PC(16:0/16:1), in CRC using imaging mass spectrometry. Specifically, elevated levels of PC(16:0/16:1) expression were observed in the more advanced stage of CRC. Our data further showed that PC(16:0/16:1) was specifically localized in the cancer region when examined using imaging mass spectrometry. Notably, because the ratio of PC(16:0/16:1) to lyso-PC(16:0) was higher in CRC, we postulated that lyso-PC acyltransferase (LPCAT) activity is elevated in CRC. In an *in vitro* analysis, we showed that LPCAT4 is involved in the deregulation of PC(16:0/16:1) in CRC. In an immunohistochemical analysis, LPCAT4 was shown to be overexpressed in CRC. These data indicate the potential usefulness of PC(16:0/16:1) for the clinical diagnosis of CRC and implicate LPCAT4 in the elevated expression of PC(16:0/16:1) in CRC. (*Cancer Sci* 2013; 104: 1295–1302)

Colorectal cancer (CRC) is the fourth most common cancer worldwide and causes approximately 600 000 deaths per year.[1] Previous studies have reported that CRC contains increased amounts of phospholipids as well as an altered phospholipid composition of the CRC cell membrane.[2,3] These changes in membrane phospholipid levels can affect cell proliferation, viability and tumor development.[2,4] Moreover, although phosphatidylcholine (PC) is the most dominant phospholipid in both non-neoplastic and cancer tissues,[5] the amount of PC is highly increased in CRC cells.[2] In addition, the changes in membrane potential and the increased PC/phosphatidylethanolamine (PE) composition rate are related to the grade of CRC malignancy.[3] In higher eukaryotes, PC is synthesized via two pathways: (i) the triple methylation of PE; and (ii) the cytidine diphosphate (CDP)-choline pathway.[6] However, the steady-state composition of PC species is maintained by the remodeling cycle (Lands' cycle).[7] The precise and concerted deacylation by phospholipase A_2 (PLA_2) and reacylation by lyso-PC acyltransferase (LPCAT) are required for normal cell functioning. Notably, the elevated expression of LPCAT1 was associated with colon cancer growth.[8] LPCAT1 is a member of the LPCAT family (LPCAT1-4) and shows LPCAT activity, preferentially incorporating palmitate into PC.[8] However, the relationship between PC remodeling and the progression of cancer, as well as the class of LPCAT involved in this process, remains unclear.

Direct mass spectrometry (MS) of biological tissue sections using matrix-assisted laser desorption/ionization (MALDI) can profile many molecules including phospholipid subtypes.[9] Furthermore, this approach can be extended to imaging MS, which can visualize the distribution of biomolecules in the tissue section.[10–13] Because specific antibodies against lipids and macromolecules are often difficult to obtain, MALDI imaging is a suitable option for detecting distinct species of these molecules directly in a tissue section. This technique has already been applied to various human cancers including prostate and gastric cancer.[14,15] Although this emerging analytical technique was initially developed as a tool for protein imaging, recently it has been increasingly used for the imaging of small organic molecules including lipids.[16] We have developed an innovative instrument that we called a mass microscope.[17] A mass microscope enables the molecules in a tissue sample to be ionized while preserving positional information regarding where the molecules have been ionized using 2-D laser scanning. The ionized molecules are analyzed using a time-of-flight (TOF)-type mass spectrometer and are presented as multiple biomolecules according to their mass-to-charge ratio (m/z). The distribution of the biomolecules is then visualized in 2-D as the signal intensity among the measurement points on the image of the tissue section.

In the present study, we applied mass microscopy to human CRC tissues as a non-targeted screening for PC biomarkers to obtain a novel molecular profile. We then performed a principal component analysis (PCA) of the data and successfully identified a difference between CRC cells and adjacent non-neoplastic colorectal mucosal cells. One PC(16:0/16:1) was visualized as differentially expressed molecules between the CRC and non-neoplastic mucosa areas. Because this PC species is known to be associated with metabolism by LPCAT families, we further specified which LPCAT (LACAT1-4) contributes to the increase in PC(16:0/16:1) in CRC.

Materials and Methods

Tissue/clinicopathological data. All samples were retrieved from the archive of Hamamatsu University Hospital. Tissue slides were evaluated histologically and graded according to the WHO classification. Cancer and corresponding non-neoplastic mucosa samples obtained from colorectal surgical specimens were snap-frozen in liquid nitrogen and stored at −80°C until required. Table 1 summarizes the clinicopathological

[8]To whom correspondence should be addressed.
E-mails: hsugimur@hama-med.ac.jp; setou@hama-med.ac.jp

doi: 10.1111/cas.12221
© 2013 Japanese Cancer Association

profiles of the samples. The study protocol was approved by the institutional review board of Hamamatsu University School of Medicine.

Sample preparation. Sample preparation was done according to the previous literature[18] and the details are in the Supporting Information.

Imaging MS analysis. All imaging MS analyses were performed using an atmospheric pressure-MALDI with a quadrupole ion trap-TOF analyser instrument, the mass microscope equipped with a diode-pumped 355 nm Nd:YAG laser (Shimadzu, Kyoto, Japan).[17] All the mass spectra were acquired using Mass Microscope System software (Shimadzu). This software consists of a graphical user interface that allows the user to specify the area to be imaged, the distance between laser shots (spatial resolution), the instrument acquisition method to be used, the number of laser shots to be irradiated at each spot and the mass range of interest to monitor. The sample was irradiated using a focused laser beam in synchrony with the stage scanning. A mass spectrum was acquired for each spot on the tissue surface. Ion images showing the localization of compounds within the sample were then obtained. The mass microscope measurements were performed in the reflection mode within a mass range of *m/z* 500–1200 using a scan pitch with a pixel size of 7.5 μm. The laser shot number and frequency were 200 per pixel and 1000 Hz, respectively. Following the imaging MS analysis, the matrix was washed with 70% ethanol and the sections were stained with H&E and photographed using a Keyence BZ-9000 (Keyence, Tokyo, Japan). The H&E-stained sections were co-registered with the imaging MS results and evaluated histologically by an experienced surgical pathologist. The lipid peak assignments were made by comparing each peak's mass measurement with the LIPID MAPS database (http://lipidmaps.org) and confirmed using MS/MS analyses (QSTAR Elite; Applied Biosystems, Foster City, CA, USA). Image reconstruction was performed using the software BioMap (freeware; www.maldi-msi.org).[19]

Data analysis and statistical analysis. Using ClinProTools 2.2 (Bruker Daltonics, Bremen, Germany), all spectra were subjected to baseline subtraction, smoothing, normalization to their own total ion current and recalibration. For each spectrum the total ion count was determined using the sum of all intensities of the spectrum. The spectra processing parameters were: baseline correction (Top Hat algorithm, minimal baseline width set to 10%); resolution (500 ppm); and smoothing (Savitzky Golay, five cycles with 2 m/z width). All spectra were recalibrated to reduce mass shifts. Peak picking was also per-

Table 1. Patient characteristics

Sex	
Male	24
Female	10
Age (years)	
<60	11
≥60	23
Mean ± SD	65.4 ± 13.1
Location	
Ascending colon	2
Transverse colon	4
Descending colon	1
Sigmoid colon	13
Rectum	14
Stage	
I	4
II	17
III	10
IV	3
Histopathological grading	
Well differentiated	20
Moderately differentiated	12
Poorly differentiated	2

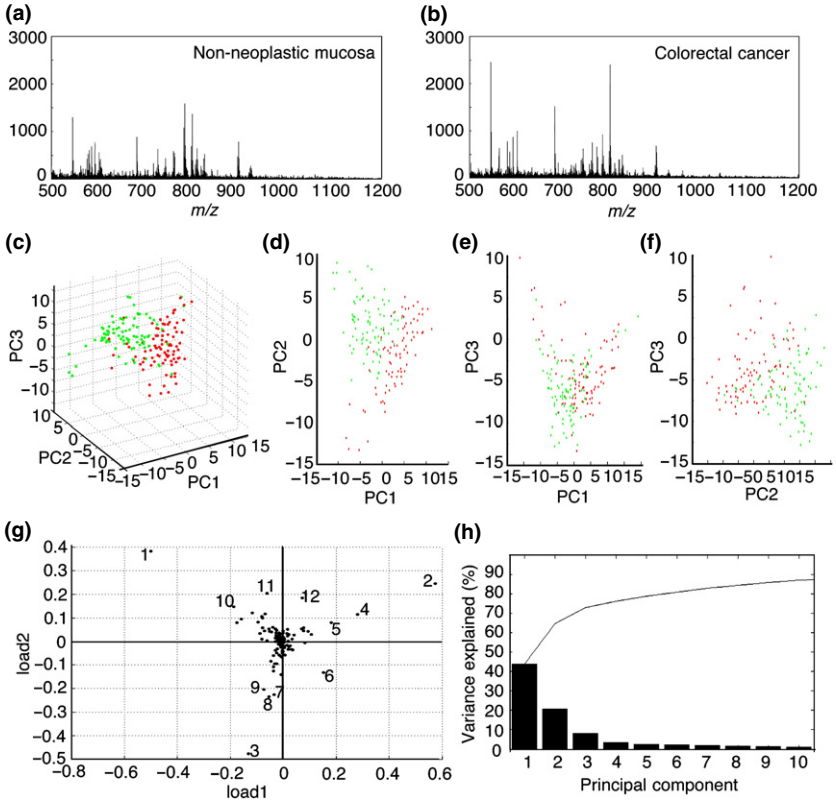

Fig. 1. Principal component analysis (PCA) of non-neoplastic mucosa and colorectal cancer (CRC). Representative mass spectra from (a) non-neoplastic mucosa and (b) CRC. (c) 3-D plotting graph of PCA. Red, CRC; green, non-neoplastic mucosa. (d–f) Corresponding 2-D graph of plotted PCA. (g) Loading plot of principal component 1 and principal component 2. The numbered components (No. 1–12) are summarized in Table 2. (h) Variance plot of principal components.

doi: 10.1111/cas.12221
© 2013 Japanese Cancer Association

Table 2. Summary of different mean peak intensities between non-cancerous mucosa and cancerous mucosa

No.†	*m/z*	Non-cancerous mucosa	Cancerous mucosa	*P*-value‡
1	798.5	68.6 ± 30.4	96.4 ± 30.1	0.0001
2	545.0	54.6 ± 20.5	34.7 ± 20.6	0.0011
3	782.5	52.1 ± 20.6	39.6 ± 21.5	0.0003
4	770.5	7.1 ± 3.2	22.5 ± 13.3	0.000001
5	546.0	20.1 ± 10.5	13.7 ± 10.6	0.0019
6	585.0	27.3 ± 10.7	14.5 ± 7.8	0.0001
7	725.5	24.1 ± 10.1	16.4 ± 10.7	0.0001
8	780.5	27.3 ± 10.8	15.9 ± 8.3	0.0001
9	783.5	23.9 ± 10.1	18.3 ± 9.6	0.0011
10	799.5	21.6 ± 9.7	33.1 ± 11.1	0.0001
11	754.5	5.7 ± 2.4	10.0 ± 3.1	0.0001
12	601.0	23.2 ± 9.1	26.7 ± 12.0	0.0707

m/z, mass-to-charge ratio. †Numbers in this column correspond to those depicted in Figure 1(g). ‡Welch's *t*-test.

formed based on the overall average spectrum over the whole mass range (signal to noise threshold of 5). Multivariate statistical analyses were performed using the supervised neural network algorithm. The pretreated data have been used for statistical analysis and visualization in ClinProTools and BioMap. There is no need for internal standards because it might interfere with the detection of isomeric endogenous lipids. The PCA was also performed using mean-centering and ClinProTools 2.2.[20,21] The stage I colorectal cancer samples were not included in the PCA analysis because these samples might interfere with the separation of the PCA plots. The PCA results were represented using two multi-dimensional plots: a score plot and a loading plot. The score plot was based on the PCA and showed similarities and differences among the samples; samples with similar peak patterns were clustered closely within the plot. The loading plot showed the influence of the data variables (in this case, the *m/z* values). The score plot of the PCA results was presented as pseudo-color images. For all the intensity calculations for the non-neoplastic mucosa and CRC, the signal intensities were generated using the ClinProt Peak Statistic Calculation and the ratio of signal intensities was then calculated. Differences in the intensities or ratios between the non-neoplastic mucosa and CRC were assessed using Welch's *t*-test.

Cell culture, transfection and cell growth. HCT116 and DLD1 cells were obtained from the American Type Culture Collection (Rockville, MD, USA). The cells were cultured in RPMI1640 medium containing 10% fetal calf serum, as described previously.[22] Before cell culture, eight-well flexiPERM slide chambers (Sarstedt, Newton, NC, USA) were attached to the poly-L-lysine-coated indium tin oxide slide glass to form culture chambers. The cells (20 000 cells/well) were then seeded onto the culture chambers. Twenty-four hours after seeding, the cells were transfected with 40 nM siRNA targeted for LPCAT1, LPCAT2, LPCAT3, LPCAT4 and a negative control using Lipofectamine 2000 (Invitrogen, Carlsbad, CA, USA). Seventy-two hours after transfection, the cells were washed twice with water and then freeze dried. The dried cells were measured using a mass microscope as described in imaging MS analysis section. Each mass intensity value is the mean ± standard error (SE) of three independent experiments. For cell growth assay, HCT116 or DLD1 cells were transfected with siRNA targeted for LPCAT4 and then seeded in a 24-well plate. Cell counting was performed every day.

RNAi and quantitative PCR (qPCR). Details are provided in the Supporting Information. Stealth RNAi oligonucleotides were used for the siRNA experiment (Invitrogen).

LPCAT assay. Details of the LPCAT assay are in the Supporting Information. 50 μg of cell lysates were add to the reaction buffer (80 mM Tris-HCl pH 7.4, 5 mM $MgCl_2$, 50 μM [^{14}C] lysopalmitoyl phosphatidylcholine and 50 μM palmitoleoyl CoA; final volume 100 μL). The reaction was incubated at 24°C for 10 min and stopped by spotting 16 μL of the reaction onto a silica, thin-layer chromatography plate (Whatman, Maidstone, UK) together with lipid standard (PC[16:0/16:1]; Avanti Polar Lipids, Alabaster, AL, USA). The plates were developed in $CHCl_3$/acetic acid/methanol/water (60/30/10/4) and the incorporation of [^{14}C] into PC was analyzed using a BIOSCAN AR-2000 (BIOSCAN, Washington, DC, USA). The standard was stained with iodine vapor.

Tissue microarray (TMA), immunohistochemistry and western blotting. Details on TMA construction and immunohistological evaluation are based on previous literature[23] and in the Supporting Information. Briefly, the expression of LPCAT4 in CRC was categorized according to the modified algorithm in previous literature, that is, the staining intensities were categorized as follows: blue (0); blue–brown (1); brown (2); and bright brown (3). The areas evaluated were a small core of the TMA (2 mm in diameter) and the apparent intratumor heterogeneity was negligible.[24–26]

Western blotting was performed as described previously.[22] β-tubulin (1:1000) was used as an internal control. Anti-LPCAT4 antibody (1:1000) was also used as a primary antibody.

Results

Unsupervised analysis distinguishes CRC from non-neoplastic mucosa. For an in-depth comparison of cancer and non-neoplastic mucosa, sections from cancer and non-neoplastic mucosa were selected and the mass spectra acquired from those regions using the mass microscope were compared to identify specific cancer markers. Tissue sections with CRC or non-neoplastic mucosa from 30 patients (Table 1) were stained with H&E to distinguish among the non-neoplastic mucosa, stroma and cancerous areas. According to the H&E-stained tissue, two quadrate areas (one from the non-neoplastic mucosa area and the other from the cancerous area) were selected to obtain mass spectra using the mass microscope. Figure 1(a,b) shows the accumulated spectra from the non-neoplastic mucosa area and the cancerous area, respectively. Both mass spectra had a large number of signals in the mass range, corresponding to the phospholipids region (*m/z*, 700–850).[27]

For the profiling experiments, spectra from each tissue were imported into the statistical analysis software ClinProTools[20,21] and a PCA was performed. The first three principal components of the CRC and non-neoplastic mucosa profiling data revealed two specific groupings capable of characterizing CRC and the non-neoplastic mucosa (Fig. 1c). Principal components 1 and 2, which describe the largest variance in the data (Fig. 1h), distinguished CRC from non-neoplastic mucosa (Fig. 1d). The CRC and non-neoplastic mucosa showed a partial overlap for principal components 2 and 3 and for principal components 1 and 3 (Fig. 1e,f). The corresponding loading plot demonstrated the influence of the *m/z* value on the respective principal components (Fig. 1g). The signal intensity of these *m/z* values from CRC and the non-neoplastic mucosa are shown in Table 2 and are numbered in order of descending loading plot absolute values (No. 1–12). A Welch's *t*-test was performed on a data set comparing CRC and the non-neoplastic mucosa. To identify CRC biomarkers, we compared the intensity of these peaks. The mean peak intensity at *m/z* 770.5 in the CRC was three times higher than that of the non-neoplastic mucosa (Table 2). Thus, we considered that the peak at *m/z* 770.5 was a major candidate for a CRC biomarker.

Product ions assignment using MS/MS and its expression in CRC. On-tissue MS/MS was used to assign the peaks. The peak at *m/z* 770.5 was identified as that of PC based on the

© 2013 Japanese Cancer Association

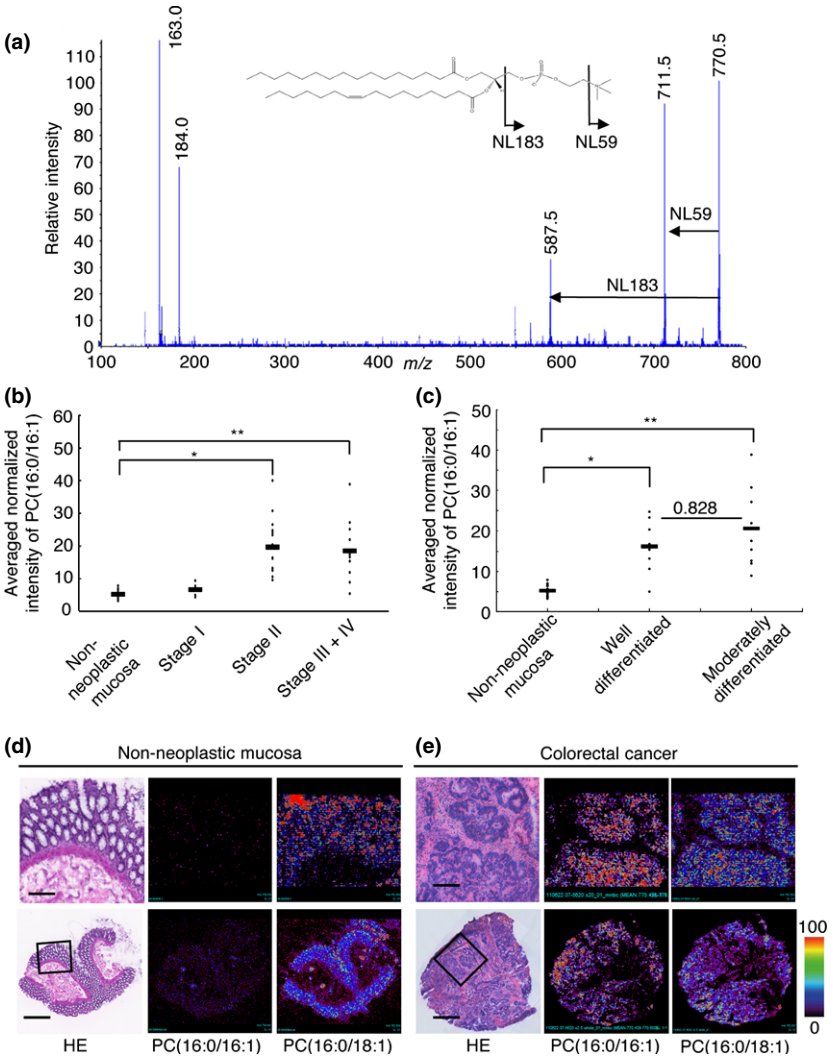

Fig. 2. The ion at the mass-to-charge ratio (*m/z*) of 770.5 can distinguish the non-neoplastic mucosa from colorectal cancer (CRC). (a) Direct MS/MS spectrum of the ion at *m/z* 770.5. The ions of the diagnostic fragments suggest that the ion at *m/z* 770.5 is that of PC(16:0/16:1). (b) Averaged normalized intensity values for PC(16:0/16:1) were plotted according to the pathological stage of CRC. The samples were analyzed using the mass microscope. The horizontal line indicates the median. $*P = 0.0027$. $**P = 0.0072$. (c) Normalized average intensity values for PC(16:0/16:1) were plotted according to the pathological differentiation state of CRC. The horizontal line indicates the median. $*P = 0.0028$. $**P = 9.3E\text{-}5$. (d, e) H&E-stained images (left) of non-neoplastic mucosa and CRC tissue and ion images showing spatial distribution of PC(16:0/16:1) (middle) and PC(16:0/18:1) (right). Bar, 150 μm (top); 600 μm (bottom). x40 (top), x2.5 (bottom). MS, mass spectrometry; NL, neutral loss; PC, phosphatidylcholine.

presence of fragment ions at an *m/z* value of 184 and a neutral loss of 59 and 183 in an MS/MS analysis, which is indicative of PC (Fig. 2a).[28,29] LIPID MAPS suggested that these peaks at *m/z* 770.5 can be assigned as $(PC[16:0/16:1]+K)^+$. Generally, PC is detected as $[M+Na]^+$ or $[M+K]^+$ ions in tissue sections; thus, the peak intensity at *m/z* 754.5 ($[PC(16:0/16:1)+Na]^+$) was compared between CRC and the non-neoplastic mucosa. We confirmed that the peak in CRC samples at *m/z* 754.5 was increased by 70% compared with those from the non-neoplastic mucosa (Table 2). In a subsequently examined section, $[M+K]^+$ ions were used to determine the intensities. To investigate the trend in PC(16:0/16:1) expression according to increasing disease stage and differentiation state of CRC, we examined the intensity of PC(16:0/16:1) in the sections. As shown in Figure 2(b,c), a significant trend toward an increased expression was observed in advanced-stage disease and every histological grade of CRC. Therefore, these results imply that PC(16:0/16:1) is a CRC-specific biomarker.

Visualization of ion images in CRC and non-neoplastic mucosa using a mass microscope. Colorectal cancer is comprised of a number of cell types, including cancerous and non-cancerous epithelial cells, non-epithelial stromal cells and infiltrating blood cells; therefore, an imaging modality such as the mass microscope is uniquely powerful for determining which areas actually contain PC(16:0/16:1). The left panel of Figure 2(d,e) shows a typical H&E stain of a thin section of non-neoplastic mucosa and CRC tissue showing regions of moderately differentiated adenocarcinoma with stromal tissues. The method allowed a parallel assessment of the histopathological features seen under a light microscope and the phospholipid profiles obtained using the mass microscope (middle and right panel of Fig. 2d,e). A comparison of the PC(16:0/16:1) signatures obtained from CRC and the non-cancerous mucosa is also shown in the middle panel of Figure 2(d,e), clearly demonstrating a cancer-specific PC(16:0/16:1) distribution. In contrast, PC(16:0/18:1) (*m/z* 782.5, $[PC(16:0/18:1)+Na]^+$) was detected in both CRC cells and non-cancerous cells (right panel of Fig. 2d,e). Therefore, use of the mass microscope enabled the imaging of a CRC biomarker *in situ*.

Involvement of LPCAT4 in the synthesis of PC(16:0/16:1). To investigate the molecular mechanism responsible for the increase in PC(16:0/16:1), we calculated the ratio of PC(16:0/16:1) to lyso-PC(16:0) (*m/z* 518.3, $[lyso\text{-}PC(16:0)+Na]^+$) in CRC and the non-neoplastic mucosa. A higher ratio of PC(16:0/16:1)/lyso-PC(16:0) was observed in CRC (Fig. 3a). This result supports the hypothesis that the conversion of lyso-PC(16:0) into PC(16:0/16:1) is activated in CRC. Recently, LPCAT (LPCAT1-4) have been described as a novel enzyme family that catalyze lyso-PC into PC[30–34] and exhibit substrate specificity for some kinds of fatty acid. If the increase in LPCAT activity in CRC is one reason for the increase in PC, the conversion of lyso-PC into PC through the catalysis of LPCAT should be elevated.[7] To examine which member of LPCAT is involved in the deregulated level of PC(16:0/16:1) *in vitro*,

doi: 10.1111/cas.12221
© 2013 Japanese Cancer Association

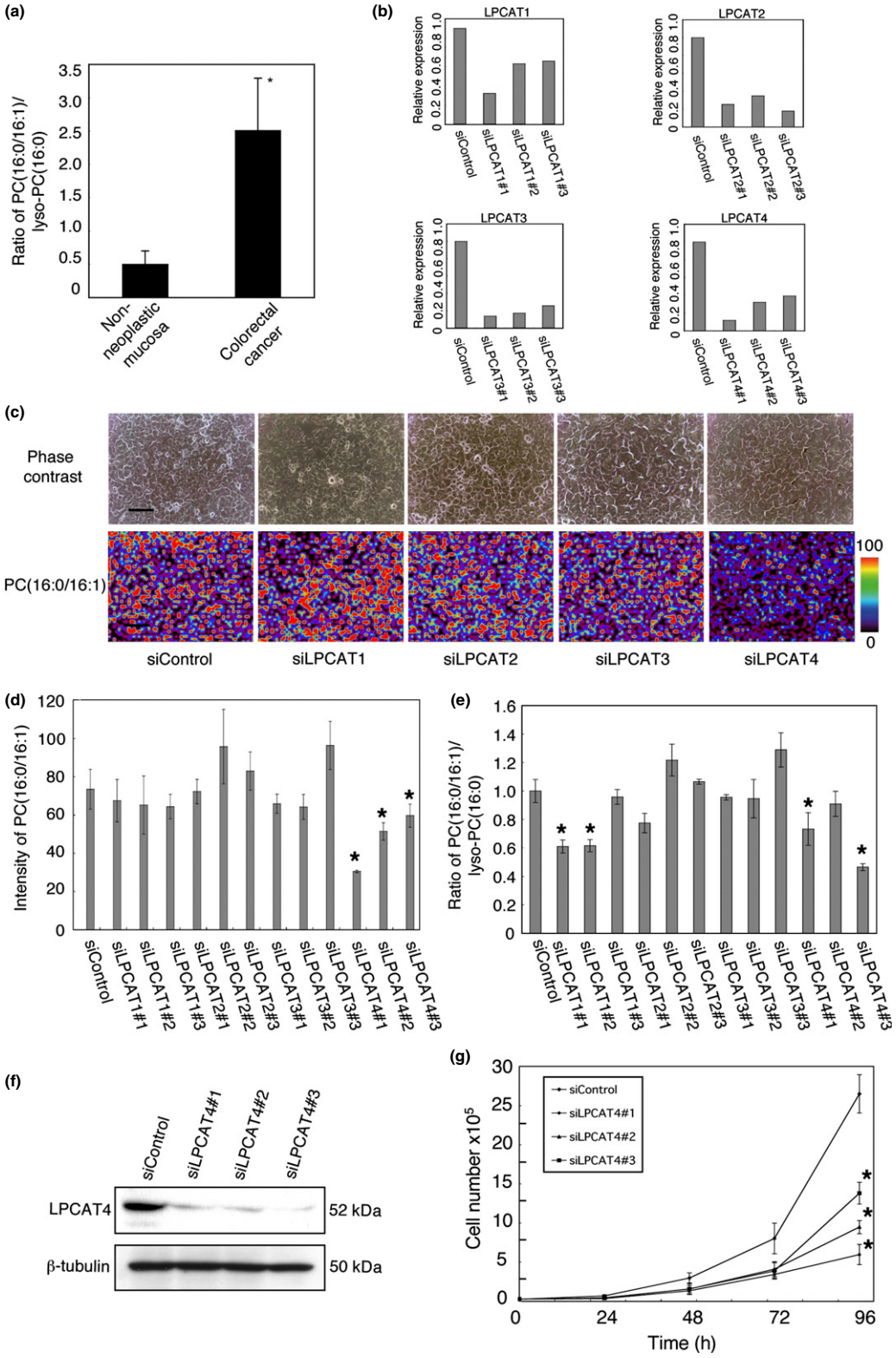

Fig. 3. Involvement of LPCAT4 in the synthesis of phosphatidylcholine (PC)(16:0/16:1) in colorectal cancer (CRC) *in vitro*. (a) The ratio of PC (16:0/16:1) to lyso-PC(16:0) was plotted for non-neoplastic mucosa and CRC. *P = 5.1E-10. (b) Efficiency of mRNA downregulation by siRNA targeted for LPCAT. The siRNA targeted for LPCAT or control siRNA were transfected into HCT116 cells. Forty-eight hours after transfection, total RNA were extracted and reverse transcription was performed. The LPCAT expression levels were quantitated using quantitative PCR. (c) Representative image of PC(16:0/16:1) in HCT116 cells analyzed using the mass microscope. Phase contrast images (top) and averaged normalized intensity images (bottom). Bar, 70 μm. (d) Effect of the downregulation of LPCAT on the averaged normalized intensity of PC(16:0/16:1). The siRNA targeted for LPCAT or control siRNA were transfected into HCT116 cells. Seventy-two hours after transfection, the cells were washed with water and then analyzed using the mass microscope. *P < 0.05. (e) LPCAT enzyme activities were analyzed using a LPCAT assay. The ratio of PC (16:0/16:1) to lyso-PC(16:0) was plotted for control and LPCAT siRNA. *P < 0.05. (f) Downregulation of LPCAT4 expression analyzed using western blotting. (g) Effect of LPCAT4 downregulation on cell growth. *P < 0.05. LPCAT, lyso-PC acyltransferase.

© 2013 Japanese Cancer Association

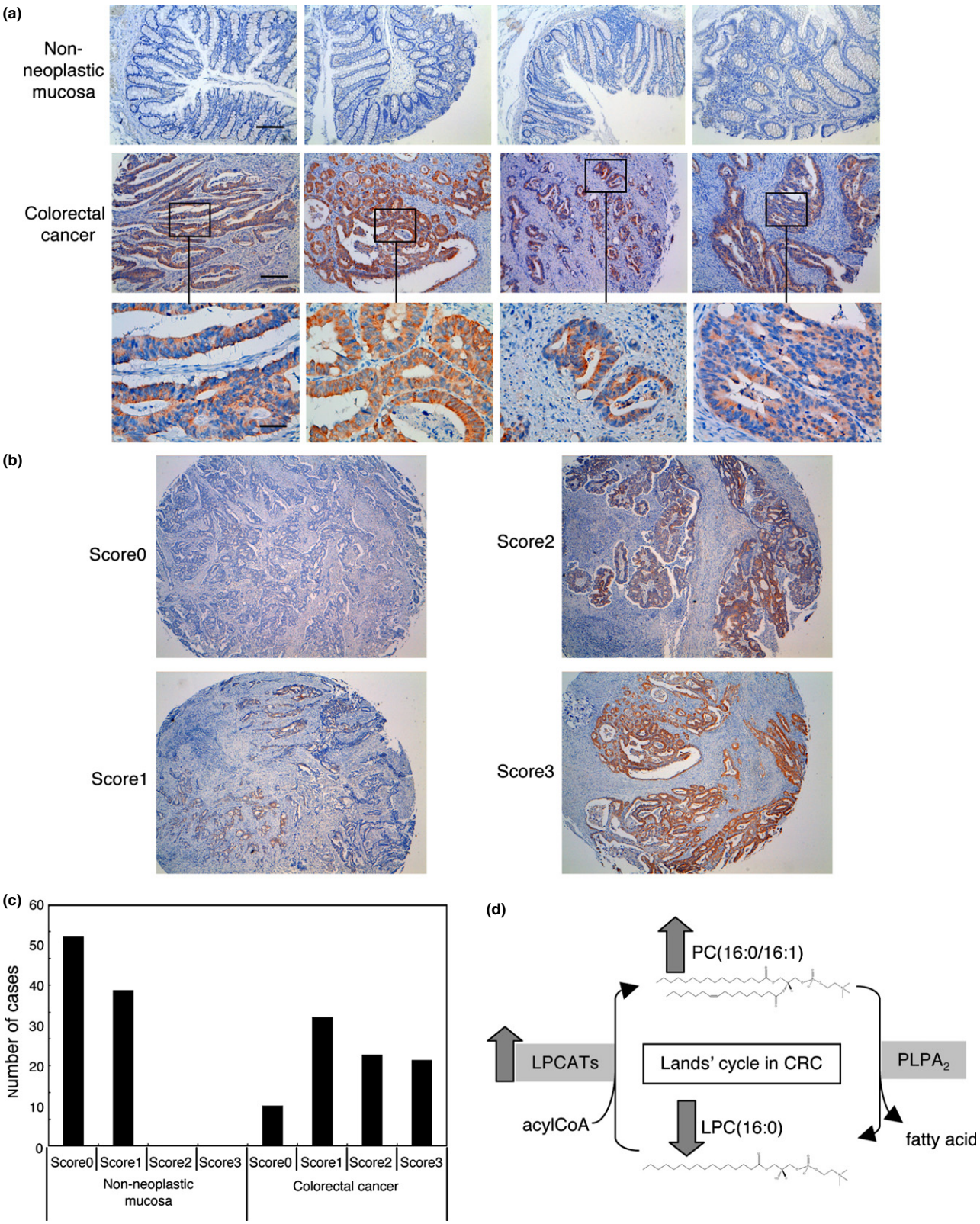

Fig. 4. Immunohistochemical analysis of the expression of LPCAT4 in a tissue microarray (TMA). (a) Non-neoplastic mucosa (top) and corresponding colorectal cancer (CRC) (middle) were stained for LPCAT4 expression using anti-LACAT4 antibody. Higher magnification images from CRC are also shown (bottom). Top, middle, ×10; bottom, ×40. Bar, 200 μm (top, middle) and 10 μm (bottom). (b) Representative scoring images. (c) Levels of LPCAT4 expression evaluated according to the scoring system described in the Materials and Methods section. The expression scores for all cases (272 cases) were examined and are presented in the graph. (d) Model of Land's cycle in CRC. LPCAT activities are elevated in CRC, which results in the increase of PC(16:0/16:1). LPCAT, lyso-PC acyltransferase.

doi: 10.1111/cas.12221
© 2013 Japanese Cancer Association

HCT116 cells were transfected with siRNA targeting LPCAT1, LPCAT2, LPCAT3 and LPCAT4. The knockdown efficiencies were evaluated using qPCR (Fig. 3b). The same experiments were also performed using DLD1 cells (Fig. S1A). The level of PC(16:0/16:1) was significantly decreased by the transfection of LPCAT4 siRNA (Fig. 3d). In DLD1 cells, the reduction of PC(16:0/16:1) was also observed in two of three LPCAT4 siRNA (Fig. S1B). The decrease in PC(16:0/16:1) was visually confirmed using the mass microscope (Fig. 3c). The LPCAT activities were analyzed using a LPCAT assay (Fig. 3e). The ratios of PC(16:0/16:1)/lyso-PC(16:0) were decreased in two of three siRNA targeted for LPCAT4. In two LPCAT1 siRNA, the ratios were also reduced. To investigate the effect of LPCAT4 expression on the growth of colon cancer cells, the cell growth was analyzed when transfected with LPCAT4 siRNA. The expression of LPCAT4 protein was significantly decreased (Fig. 3f). The knockdown of LPCAT4 caused delayed growth (Figs 3g, S1C). In Figure S1(C), cell growth was not inhibited by the transfection of siRNA targeted for LPCAT1 (siLPCAT1#1), which is likely because of the off-target effect of siRNA. To further confirm the involvement of LPCAT4 in CRC progression, we examined the expression of LPCAT4 immunohistochemically. A total of 272 tissue samples (136 benign and 136 CRC; Table S1) were stained for LPCAT4 expression and a total of 100 adenomas (Table S2) were also analyzed. LPCAT4 immunoreactivity was stronger in CRC than in the non-tumor mucosa and its expression seems to be in the endoplasmic reticulum in the cytoplasm (Fig. 4a). Stromal cells were not stained with LPCAT4 antibody. The stainings with four defined categories are shown in Figure 4(b). When immunohistochemical scores greater than 2 were considered, LPCAT4 was upregulated in 69% of the CRC samples (Fig. 4c). In contrast, the non-neoplastic mucosa displayed little or no LPCAT4 expression. Adenomas also had little staining with the LPCAT4 antibody (Fig. S2). The correlation between PC(16:0/16:1) expression measured using the mass microscope and the immunohistochemical score is shown in Table S3.

Discussion

In the present study, direct-tissue profiling using imaging MS was used to analyze the phospholipid patterns within human CRC and non-neoplastic colorectal mucosa. One of the unique starting points of the present study was the use of primary human cancer tissues, which are often difficult to handle, in the search for cancer biomarkers that have escaped previous investigators' attempts at identification. A PCA of the total mass spectra revealed separate clusters for CRC and the non-neoplastic mucosa (Fig. 1). According to the PCA and the corresponding loading plots, the *m/z* values that contributed to the separation of each group could be identified (Table 2). We also showed that the *m/z* value from the phospholipid PC(16:0/16:1) was differentially expressed in CRC and the non-neoplastic mucosa.

In the present study, a phospholipid analysis of CRC samples using imaging MS showed differences between CRC and the non-neoplastic mucosa (Fig. 2). PC(16:0/16:1) was specifically localized in CRC areas, demonstrating that PC(16:0/16:1) is a CRC marker. Thus, PC(16:0/16:1) is a novel CRC-specific biomarker. The simultaneous characterization of molecular information and histological structures using imaging MS is very useful in various clinicopathological settings, as previously reported by our group.[35–37] Currently, the mass microscope is the most powerful modality for identifying lipids. Consequently, imaging MS has the ability to overcome some of the weaknesses of immunohistochemistry. Direct analysis of the metabolome in cancer tissues could provide a more precise representation in tissues than that provided using other methods currently used in the field of pathology.

To investigate LPCAT activity in the present study, we examined the PC(16:0/16:1) and lyso-PC(16:0) cell membrane constituents. The ratio of PC(16:0/16:1)/lyso-PC(16:0) in CRC was higher than that in the non-neoplastic mucosa (Fig. 3a). The ratio was reduced when HCT116 cells were transfected with siRNA targeted for LPCAT1 and LPCAT4 (Fig. 3e). Therefore, this result supports the catalytic activation of LPCAT in CRC cells. Notably, the silencing of LPCAT4 reduced the PC(16:0/16:1) level and cell growth in the colon cancer cell line HCT116 and DLD1 *in vitro* (Figs 3d, S1B). Moreover, LPCAT4 was overexpressed in CRC (Fig. 4). LPCAT4 (also named MBOAT2) is one of the four mammalian LPCAT that have been cloned[33] and plays a catalytic role with a preference for fatty acid (FA)(16:1) and FA(18:1) in PC synthesis.[33,34] This finding suggests that enhanced reacylation of lyso-PC by LPCAT alters the amount of PC(16:0/16:1) in cancer cell membranes. The different influences of these four classes of the LPCAT family on human cancer cell characteristics have only been elucidated recently. The upregulation of LPCAT1 stimulated cell growth in the colon cancer cell line SW480.[8] Meanwhile, the knockdown of LPCAT3 by siRNA induced apoptosis and morphological changes in HEK293 cells.[38] Thus, LPCAT are involved in several aspects of tumorigenesis. Figure 4(d) is a model of PC(16:0/16:1) synthesys in CRC. In CRC, LPCAT activity is thought to be elevated, which results in increased production of PC(16:0/16:1).

We demonstrated that imaging MS can distinguish CRC from non-neoplastic mucosa based on their biomolecular signatures and can be used to identify phospholipid biomarkers. We showed that LPCAT4 contributes to PC(16:0/16:1) accumulation in CRC via the enhanced reacylation of lyso-PC. Further studies are necessary to conclude whether LPCAT4 is the sole factor responsible for the increase of PC(16:0/16:1) in CRC.

Acknowledgments

The authors are grateful to Hisaki Igarashi at the Department of Tumor Pathology, Hamamatsu University School of Medicine, for his excellent technical assistance in the cryostat sectioning. This work was supported by Grants-in-Aid (Research on International Cooperation in Medical Science, Grants-in-Aid for Cancer Research, 21-1) from the Ministry of Health, Labour and Welfare, the Japan Society for the Promotion of Science (22590356, 22790378, 23116510 and 20670004), the Ministry of Education, Culture, Sports, Science and Technology (221S0001), the Princess Takamatsu Cancer Research Foundation and the Smoking Research Foundation of Japan.

Disclosure Statement

The authors have no conflict of interest.

References

1 Boyle P, Levin B. *World Cancer Report 2008*. Lyon Cedex, France: WHO Press, 2008.

2 Dueck DA, Chan M, Tran K *et al.* The modulation of choline phosphoglyceride metabolism in human colon cancer. *Mol Cell Biochem* 1996; **162**: 97–103.

3 Dobrzynska I, Szachowicz-Petelska B, Sulkowski S, Figaszewski Z. Changes in electric charge and phospholipids composition in human colorectal cancer cells. *Mol Cell Biochem* 2005; **276**: 113–9.

4 Preetha A, Banerjee R, Huilgol N. Surface activity, lipid profiles and their implications in cervical cancer. *J Cancer Res Ther* 2005; **1**: 180–6.

© 2013 Japanese Cancer Association

5 White DA. The phospholipids composition of mammalian tissues. In: Ansell GB, Hawthorne JN, Dawson RMC, eds. *Form and Function of Phospholipids*. Amsterdam: Elsevier, 1973; 441–82.
6 Bishop WR, Bell RM. Assembly of phospholipids into cellular membranes: biosynthesis, transmembrane movement and intracellular translocation. *Annu Rev Cell Biol* 1988; **4**: 579–610.
7 Shindou H, Hishikawa D, Harayama T, Yuki K, Shimizu T. Recent progress on acyl CoA: lysophospholipid acyltransferase research. *J Lipid Res* 2009; **50**(Suppl.): S46–51.
8 Mansilla F, da Costa KA, Wang S *et al.* Lysophosphatidylcholine acyltransferase 1 (LPCAT1) overexpression in human colorectal cancer. *J Mol Med (Berl)* 2009; **87**: 85–97.
9 Woods AS, Jackson SN. Brain tissue lipidomics: direct probing using matrix-assisted laser desorption/ionization mass spectrometry. *AAPS J* 2006; **8**: E391–5.
10 McDonnell LA, Heeren RM. Imaging mass spectrometry. *Mass Spectrom Rev* 2007; **26**: 606–43.
11 Chaurand P, Sanders ME, Jensen RA, Caprioli RM. Proteomics in diagnostic pathology: profiling and imaging proteins directly in tissue sections. *Am J Pathol* 2004; **165**: 1057–68.
12 Cornett DS, Reyzer ML, Chaurand P, Caprioli RM. MALDI imaging mass spectrometry: molecular snapshots of biochemical systems. *Nat Methods* 2007; **4**: 828–33.
13 Seeley EH, Caprioli RM. Molecular imaging of proteins in tissues by mass spectrometry. *Proc Natl Acad Sci U S A* 2008; **105**: 18126–31.
14 Cazares LH, Troyer D, Mendrinos S *et al.* Imaging mass spectrometry of a specific fragment of mitogen-activated protein kinase/extracellular signal-regulated kinase kinase kinase 2 discriminates cancer from uninvolved prostate tissue. *Clin Cancer Res* 2009; **15**: 5541–51.
15 Morita Y, Ikegami K, Goto-Inoue N *et al.* Imaging mass spectrometry of gastric carcinoma in formalin-fixed paraffin-embedded tissue microarray. *Cancer Sci* 2010; **101**: 267–73.
16 Liu Y, Chen Y, Momin A *et al.* Elevation of sulfatides in ovarian cancer: an integrated transcriptomic and lipidomic analysis including tissue-imaging mass spectrometry. *Mol Cancer* 2010; **9**: 186.
17 Harada T, Yuba-Kubo A, Sugiura Y *et al.* Visualization of volatile substances in different organelles with an atmospheric-pressure mass microscope. *Anal Chem* 2009; **81**: 9153–7.
18 Kurabe N, Hayasaka T, Igarashi H *et al.* Visualization of phosphatidylcholine (16:0/16:0) in type II alveolar epithelial cells in the human lung using imaging mass spectrometry. *Pathol Int* 2013; **63**: 195–200.
19 Shimma S, Sugiura Y, Hayasaka T, Zaima N, Matsumoto M, Setou M. Mass imaging and identification of biomolecules with MALDI-QIT-TOF-based system. *Anal Chem* 2008; **80**: 878–85.
20 Deininger SO, Ebert MP, Futterer A, Gerhard M, Rocken C. MALDI imaging combined with hierarchical clustering as a new tool for the interpretation of complex human cancers. *J Proteome Res* 2008; **7**: 5230–6.
21 Willems SM, van Remoortere A, van Zeijl R, Deelder AM, McDonnell LA, Hogendoorn PC. Imaging mass spectrometry of myxoid sarcomas identifies proteins and lipids specific to tumour type and grade, and reveals biochemical intratumour heterogeneity. *J Pathol* 2010; **222**: 400–9.
22 Kahyo T, Iwaizumi M, Shinmura K *et al.* A novel tumor-derived SGOL1 variant causes abnormal mitosis and unstable chromatid cohesion. *Oncogene* 2011; **30**: 4453–63.
23 Sugimura H, Mori H, Nagura K *et al.* Fluorescence in situ hybridization analysis with a tissue microarray: 'FISH and chips' analysis of pathology archives. *Pathol Int* 2010; **60**: 543–50.
24 Okudela K, Yazawa T, Ishii J *et al.* Down-regulation of FXYD3 expression in human lung cancers: its mechanism and potential role in carcinogenesis. *Am J Pathol* 2009; **175**: 2646–56.
25 Costa WH, Rocha RM, Cunha IW, Guimaraes GC, Zequi Sde C. Immunohistochemical expression of CD44s in renal cell carcinoma lacks independent prognostic significance. *Int Braz J Urol* 2012; **38**: 456–65.
26 Natsume H, Shinmura K, Tao H *et al.* The CRKL gene encoding an adaptor protein is amplified, overexpressed, and a possible therapeutic target in gastric cancer. *J Transl Med* 2012; **10**: 97.
27 Garrett TJ, Yost RA. Analysis of intact tissue by intermediate-pressure MALDI on a linear ion trap mass spectrometer. *Anal Chem* 2006; **78**: 2465–9.
28 Hayasaka T, Goto-Inoue N, Sugiura Y *et al.* Matrix-assisted laser desorption /ionization quadrupole ion trap time-of-flight (MALDI-QIT-TOF)-based imaging mass spectrometry reveals a layered distribution of phospholipid molecular species in the mouse retina. *Rapid Commun Mass Spectrom* 2008; **22**: 3415–26.
29 Al-Saad KA, Siems WF, Hill HH, Zabrouskov V, Knowles NR. Structural analysis of phosphatidylcholines by post-source decay matrix-assisted laser desorption/ionization time-of-flight mass spectrometry. *J Am Soc Mass Spectrom* 2003; **14**: 373–82.
30 Chen X, Hyatt BA, Mucenski ML, Mason RJ, Shannon JM. Identification and characterization of a lysophosphatidylcholine acyltransferase in alveolar type II cells. *Proc Natl Acad Sci U S A* 2006; **103**: 11724–9.
31 Shindou H, Hishikawa D, Nakanishi H *et al.* A single enzyme catalyzes both platelet-activating factor production and membrane biogenesis of inflammatory cells. Cloning and characterization of acetyl-CoA:LYSO-PAF acetyltransferase. *J Biol Chem* 2007; **282**: 6532–9.
32 Zhao Y, Chen YQ, Bonacci TM *et al.* Identification and characterization of a major liver lysophosphatidylcholine acyltransferase. *J Biol Chem* 2008; **283**: 8258–65.
33 Hishikawa D, Shindou H, Kobayashi S, Nakanishi H, Taguchi R, Shimizu T. Discovery of a lysophospholipid acyltransferase family essential for membrane asymmetry and diversity. *Proc Natl Acad Sci U S A* 2008; **105**: 2830–5.
34 Gijon MA, Riekhof WR, Zarini S, Murphy RC, Voelker DR. Lysophospholipid acyltransferases and arachidonate recycling in human neutrophils. *J Biol Chem* 2008; **283**: 30235–45.
35 Hayasaka T, Goto-Inoue N, Ushijima M *et al.* Development of imaging mass spectrometry (IMS) dataset extractor software. IMS convolution. *Anal Bioanal Chem* 2011; **401**: 183–93.
36 Setou M. *Imaging Mass Spectrometry: Protocols for Mass Microscopy*, 1st edn. Tokyo, Japan: Springer, 2010.
37 Setou M, Kurabe N. Mass microscopy: high-resolution imaging mass spectrometry. *J Electron Microsc (Tokyo)* 2011; **60**: 47–56.
38 Jain S, Zhang X, Khandelwal PJ, Saunders AJ, Cummings BS, Oelkers P. Characterization of human lysophospholipid acyltransferase 3. *J Lipid Res* 2009; **50**: 1563–70.

Supporting Information

Additional Supporting Information may be found in the online version of this article:

Fig. S1. Involvement of LPCAT4 in the synthesis of PC(16:0/16:1) in DLD1 *in vitro.*

Fig. S2. Immunohistochemical analysis of the expression of LPCAT4 in adenomatous polyp.

Table S1. Clinicopathological profile of the cases on tissue microarray.

Table S2. Clinicopathological profile of polyps.

Table S3. Correlation of intensities generated using a mass microscope and immunohistochemical score.

Supplementary Methods. Including: LPCAT assay; immunohistochemistry; RNAi; and RT-PCR.

doi: 10.1111/cas.12221
© 2013 Japanese Cancer Association